Proceedings of the ASME 2010 3rd Joint US-European Fluids Engineering Summer Meeting and 8th International Conference on Nanochannels, Microchannels, and Minichannels
FEDSM-ICNMM2010
August 1-5, 2010, Montreal, Canada

FEDSM-ICNMM2010-31228

Convective Stability of Hadley Circulations in finite domains

P.N. Kaloni **J.X. Lou**
Department of Mathematics and Statistics
University of Windsor, Windsor, Ontario, Canada N9B 3P4

ABSTRACT

We present numerical solutions of natural convection in a cavity of finite domain when the flow is driven by a horizontal temperature gradient between isothermal vertical walls. Only the transverse roll structure of convection is calculated by employing the pseudo spectral Chebyshev collocation method. A numerical solution of the steady flow is first obtained and, based upon it, the critical Rayleigh number (related to Grashof number) of linear transverse mode is determined. The influence of aspect ratio, on the flow and temperature patterns, is also investigated.

1 Introduction

The problem of natural convection in a closed shallow cavity, with an imposed horizontal temperature gradient, has been considered by serval authors. The work on stability was begun by Hart[1, 2] who noted that when the fluid in heated differentially at the two ends of the cavity, a unicellular flow is established. Such single cell flows have become known as Hadley circulations, after the pioneering work of Hadley[3] in geophysics. Besides finding applications in planetary atmosphere, such shallow cavity flows have applications in growing of semi conductor crystals, cooling of gas-cooled reactor, dispersion of pollutants in river estuaries and motion in storm windows.

Subsequent extensions and improvements to Harts' work have been considered by Kuo and Korpela[4], Wang and Korpela[5], Laure and Roux[6] and many others. Daniels, Blythe and Simpkins[7] consider the flow near the vertical walls of the cavity and discuss the possibilities of the onset of multicellular convection. Most of these studies, however, consider the ratio of the height to other two dimensions to be considerably small. Moreover, because of the applications in liquid metals, a number of these studies deal with low Prandtl number fluid only. Experimental investigation of cavity flows, driven by lateral heating, have been reported by Imberger[8], Ostrach, Loka and Kumer[9], Simpkins and Dudderar[10] and Hung and Andreck[11]. Generally, these consist of a main circulation in which the fluid motion is up along the hot wall, across the top, down at the cold wall and returning across the bottom.

Drummond and Korpela[12] have presented numerical results in shallow cavities for a certain range of Grashof number, and for Prandtl number $Pr < 2.0$. Their calculations are based on the time integration technique, using finite difference method. Cormack, Leal and Steinfeld[13] also present numerical solutions for natural convection for closed cavity problem with small aspect ratio. These authors consider various limiting cases by employing the standard methods of matched asymptotic expansions. They find that heat is mainly transferred by conduction when the Grashof number is quite low. Park and Ryu[14] used the Chebyshev pseudo-spectral collocation method for Rayleigh-Benard convection of viscoelastic fluids in finite domains.

In the present paper we employ a Chebyshev pseudo-spectral collocation method to study the title problem at a fixed Prandtl number and focus only on the transverse mode. We consider the effect of varying the aspect ratio and horizontal Rayleigh number, in stream lines, iso-streamline patterns, isotherms etc. Since only transverse modes are considered, the problem can be considered as two-dimensional one.

2 Governing Equations

Consider a cavity, as shown in Fig. 1. The fluid is confined within a finite domain. A Cartesian coordinate system (x, y, z) is chosen such that origin is in the middle of the layer and z-axis is vertically upward. The fluid layer is taken to be confined in a cavity to be large in its y direction and small of the thickness d_z in the z direction,

and of moderate thickness d_x in the x direction. It is also assumed that the ratio of d_x or d_z to the length in the y direction is considerably small so that the lateral end effects do not influence the motion in the central part. The problem thus may be considered as two dimensional problem.

We non-dimensionalize the quantities as follows:

$$\beta = \frac{d_x}{d_z},\ \ t = \frac{\kappa \tilde{t}}{{d_z}^2},\ \ x = 2\frac{\tilde{x}}{d_x} = 2\frac{\tilde{x}}{\beta d_z},\ \ z = 2\frac{\tilde{z}}{d_z},$$
$$u = \frac{d_z \tilde{u}}{\kappa},\ \ w = \frac{d_z \tilde{w}}{\kappa},\ \ p = \frac{d_z^2}{\eta\kappa}\tilde{p},\ \ Pr = \frac{\eta}{\kappa\rho_0},$$
$$R_H = \frac{g\alpha {d_z}^3 \rho_0 \Delta T}{\beta\eta\kappa},\ \ T = \frac{\eta\kappa}{g\alpha {d_z}^3 \rho_0}\tilde{T}$$

where coordinate vector $\tilde{x} = (\tilde{x}, 0, \tilde{z})$, velocity vector $\tilde{v} = (\tilde{u}, 0, \tilde{w})$, g is the gravitational constant, Pr is the Prandtl number, R_H is the Rayleigh number, which is equivalent to the Grashof number multiplied by the Prandtl number. ρ_0 is the density, T the temperature, α the coefficient of thermal expansion, η is the fluid viscosity and κ the thermal diffusivity. β is the ratio of length in x direction to z direction, ΔT is the temperature difference between two walls $x = 1$ and $x = -1$.

On using Boussinesq approximation, the non dimensional governing equations then take the form:

$$\frac{1}{\beta}\frac{\partial u}{\partial x} + \frac{\partial w}{\partial z} = 0, \tag{1}$$

$$\frac{1}{Pr}\left(\frac{\partial u}{\partial t} + 2u\frac{1}{\beta}\frac{\partial u}{\partial x} + 2w\frac{\partial u}{\partial z}\right) = -2\frac{1}{\beta}\frac{\partial p}{\partial x} + \frac{4}{\beta^2}\frac{\partial^2 u}{\partial x^2} + 4\frac{\partial^2 u}{\partial z^2}, \tag{2}$$

$$\frac{1}{Pr}\left(\frac{\partial w}{\partial t} + 2u\frac{1}{\beta}\frac{\partial w}{\partial x} + 2w\frac{\partial w}{\partial z}\right) = -2\frac{\partial p}{\partial z} + \frac{4}{\beta^2}\frac{\partial^2 w}{\partial x^2} + 4\frac{\partial^2 w}{\partial z^2} + T, \tag{3}$$

$$\frac{\partial T}{\partial t} + 2u\frac{1}{\beta}\frac{\partial T}{\partial x} + 2w\frac{\partial T}{\partial z} = +\frac{4}{\beta^2}\frac{\partial^2 T}{\partial x^2} + 4\frac{\partial^2 T}{\partial z^2}, \tag{4}$$

and the corresponding non dimensional forms of boundary conditions become:

$$u = w = 0,\quad T = -\frac{1}{2}\beta R_H x \quad at \quad z = \pm 1; \tag{5}$$

$$u = w = 0,\quad T = \mp\frac{1}{2}\beta R_H \quad at \quad x = \pm 1. \tag{6}$$

For simplicity, we denote the stream function by φ and using the following form for temperature variable θ.

$$u = -2\frac{\partial \varphi}{\partial z},\quad w = \frac{2}{\beta}\frac{\partial \varphi}{\partial x},\quad T = -\frac{1}{2}R_H x + \theta. \tag{7}$$

The equations in φ and θ are transformed into:

$$-\frac{4}{Pr}\frac{\partial}{\partial t}\left(\frac{1}{\beta^2}\frac{\partial^2\varphi}{\partial x^2} + \frac{\partial^2\varphi}{\partial z^2}\right) - R_H + \frac{2}{\beta}\frac{\partial\theta}{\partial x} + \frac{16}{\beta^4}\frac{\partial^4\varphi}{\partial x^4} + 16\frac{\partial^4\varphi}{\partial z^4} + \frac{32}{\beta^2}\frac{\partial^4\varphi}{\partial x^2\partial z^2} + \frac{16}{Pr\beta}\frac{\partial\varphi}{\partial z}\frac{\partial^3\varphi}{\partial x\partial z^2} - \frac{16}{Pr\beta}\frac{\partial\varphi}{\partial x}\frac{\partial^3\varphi}{\partial z^3} + \frac{16}{Pr\beta^3}\frac{\partial\varphi}{\partial z}\frac{\partial^3\varphi}{\partial x^3} - \frac{16}{Pr\beta^3}\frac{\partial\varphi}{\partial x}\frac{\partial^3\varphi}{\partial x^2\partial z} = 0, \tag{8}$$

$$\frac{\partial\theta}{\partial t} + 2R_H\frac{\partial\varphi}{\partial z} - 4\frac{1}{\beta^2}\frac{\partial^2\theta}{\partial x^2} - 4\frac{\partial^2\theta}{\partial z^2} - 4\frac{1}{\beta}\frac{\partial\varphi}{\partial z}\frac{\partial\theta}{\partial x} + 4\frac{1}{\beta}\frac{\partial\varphi}{\partial x}\frac{\partial\theta}{\partial z} = 0, \tag{9}$$

and corresponding boundary conditions become:

$$\varphi = \frac{\partial\varphi}{\partial x} = \theta = 0,\quad at \quad x = \pm 1; \tag{10}$$

$$\varphi = \frac{\partial\varphi}{\partial z} = \theta = 0,\quad at \quad z = \pm 1. \tag{11}$$

We now split the variables φ and θ into the steady and perturb parts, and perform the standard normal mode analysis. We denote the steady-state solutions as (φ^s, θ^s) and fluctuating solutions as (φ', θ') and write:

$$\varphi(x,z,t) = \varphi^s(x,z) + \varphi'(x,z) * \exp(\sigma t), \tag{12}$$

$$\theta(x,z,t) = \theta^s(x,z) + \theta'(x,z) * \exp(\sigma t). \tag{13}$$

On substituting the expression (12) and (13) into equations (8) and (9) and separating the resulting equations for the steady and fluctuating parts, we have:

$$\boldsymbol{\mathcal{L}}_1 = -R_H + \frac{2}{\beta}\frac{\partial\theta^s}{\partial x} + \frac{16}{\beta^4}\frac{\partial^4\varphi^s}{\partial x^4} + 16\frac{\partial^4\varphi^s}{\partial z^4} + \frac{32}{\beta^2}\frac{\partial^4\varphi^s}{\partial x^2\partial z^2} + \frac{16}{Pr\beta}\frac{\partial\varphi^s}{\partial z}\frac{\partial^s\varphi^s}{\partial x\partial z^2} - \frac{16}{Pr\beta}\frac{\partial\varphi^s}{\partial x}\frac{\partial^3\varphi^s}{\partial z^3} + \frac{16}{Pr\beta^3}\frac{\partial\varphi^s}{\partial z}\frac{\partial^3\varphi^s}{\partial x^3} - \frac{16}{Pr\beta^3}\frac{\partial\varphi^s}{\partial x}\frac{\partial^3\varphi^s}{\partial x^2\partial z} = 0,$$

$$\boldsymbol{\mathcal{L}}_2 = 2R_H\frac{\partial\varphi^s}{\partial z} - 4\frac{1}{\beta^2}\frac{\partial^2\theta^s}{\partial x^2} - 4\frac{\partial^2\theta^s}{\partial z^2} - 4\frac{1}{\beta}\frac{\partial\varphi^s}{\partial z}\frac{\partial\theta^s}{\partial x} + 4\frac{1}{\beta}\frac{\partial\varphi^s}{\partial x}\frac{\partial\theta^s}{\partial z} = 0, \tag{14}$$

and

$$\boldsymbol{\mathcal{E}}_1 = -\frac{4}{Pr}(\frac{1}{\beta^2}\frac{\partial^2\varphi'}{\partial x^2} + \frac{\partial^2\varphi'}{\partial z^2})\sigma + \frac{2}{\beta}\frac{\partial\theta'}{\partial x} + \frac{16}{\beta^4}\frac{\partial^4\varphi'}{\partial x^4} + \frac{32}{\beta^2}\frac{\partial^4\varphi'}{\partial x^2\partial z^2} + 16\frac{\partial^4\varphi'}{\partial z^4} + \frac{16}{Pr\beta^3}\frac{\partial\varphi'}{\partial z}\frac{\partial^3\varphi^s}{\partial x^3} - \frac{16}{Pr\beta^3}\frac{\partial\varphi'}{\partial x}\frac{\partial^3\varphi^s}{\partial x^2\partial z} - \frac{16}{Pr\beta^3}\frac{\partial\varphi^s}{\partial x}\frac{\partial^3\varphi'}{\partial x^2\partial z} + \frac{16}{Pr\beta^3}\frac{\partial\varphi^s}{\partial z}\frac{\partial^3\varphi'}{\partial x^3} - \frac{16}{Pr\beta}\frac{\partial\varphi^s}{\partial x}\frac{\partial^3\varphi'}{\partial z^3} - \frac{16}{Pr\beta}\frac{\partial\varphi'}{\partial x}\frac{\partial^3\varphi^s}{\partial z^3} + \frac{16}{Pr\beta}\frac{\partial\varphi^s}{\partial z}\frac{\partial^3\varphi'}{\partial x\partial z^2} + \frac{16}{Pr\beta}\frac{\partial\varphi'}{\partial z}\frac{\partial^3\varphi^s}{\partial x\partial z^2} = 0,$$

$$\boldsymbol{\mathcal{E}}_2 = \theta'\sigma + 2R_H\frac{\partial\varphi'}{\partial z} - \frac{4}{\beta^2}\frac{\partial^2\theta'}{\partial x^2} - 4\frac{\partial^2\theta'}{\partial z^2} - \frac{4}{\beta}\frac{\partial\varphi^s}{\partial z}\frac{\partial\theta'}{\partial x} - \frac{4}{\beta}\frac{\partial\varphi'}{\partial z}\frac{\partial\theta^s}{\partial x} + \frac{4}{\beta}\frac{\partial\varphi^s}{\partial x}\frac{\partial\theta'}{\partial z} + \frac{4}{\beta}\frac{\partial\varphi'}{\partial x}\frac{\partial\theta^s}{\partial z} = 0. \tag{15}$$

Both sets φ^s, θ^s and φ',θ' should satisfy the boundary conditions:

$$\varphi^s = \frac{\partial \varphi^s}{\partial x} = \theta^s = 0, \; at \quad x = \pm 1 \; and \; z = \pm 1; \tag{16}$$

$$\varphi' = \frac{\partial \varphi'}{\partial z} = \theta' = 0, \; at \; x = \pm 1 \; and \; z = \pm 1. \tag{17}$$

3 Chebyshev pseudo-spectral method

The solution of differential equations by the Chebyshev pseudo-spectral method[15] is based on the representation of the derivative operators, d/dx and d^2/dx^2, in a discrete ordinate basis. The Chebyshev polynomials $T_k(x)$ are orthogonal with respect to the weight function $w(x) = (1-x^2)^{-1/2}$, that is,

$$\int_1^1 w(x) T_K(x) T_L(x) dx = \frac{c_k}{2} \pi \delta_{K,L}, \tag{18}$$

where

$$T_k(x) = \cos(k \arccos x),$$
$$-1 \le x \le 1, \quad k = 0, 1, 2, \ldots, \tag{19}$$

and $c_0 = 2, c_i = 1 (i \ge 1)$. The Gauss-Lobatto integration involves the evaluation of an integral by a finite sum, given by:

$$\int_1^1 w(x) f(x) dx = \sum_{i=0}^{L} w_i f(x_i), \tag{20}$$

where $w_i = \frac{\pi}{c_i L}$ are the weights and $x_i = -\cos\frac{i\pi}{L}$ are the roots of derivatives of Chebyshev polynomials. as Gauss-Lobatto collocation (GLC) points. The collocation method is based on the representation of a function by its values at $L+1$ root points, i.e., $f(x_i)$. We expand the function in Chebyshev polynomials

$$f(x) = \sum_{k=0}^{L} a_k T_k(x), \tag{21}$$

where a_k are the expansion coefficients given by

$$a_k = \frac{2}{c_k \pi} \int_{-1}^{1} w(x) f(x) T_k(x) dx. \tag{22}$$

If we substitute (22) into (21) and apply the Gauss-Lobatto integration formula (20), it allows us to construct the interpolation formula, that is

$$f(x) = \sum_{j=0}^{L} g_j(x) f(x_j), \tag{23}$$

where the interpolating polynomial is given by

$$g_j(x) = \frac{2}{L c_j} \sum_{k=0}^{L} \frac{1}{c_k} T_k(x_j) T_k(x). \tag{24}$$

After introducing the Gauss-Lobatto integration, the c_j in (18) and (24) will be $c_0 = c_L = 2$, $c_j = 1, for \, 1 \le j \le L$. Equation (23) implies that the derivative of $f(x)$ can be represented by derivatives of the interpolating polynomials $g_i(x)$ given by (24).

Two dimensional function $f(x,z)$, defined for $-1 \le x \le 1$ and $-1 \le z \le 1$, and based at Gauss-Lobatto collocation points $x_i = -\cos(\frac{i\pi}{L_x}), 0 \le i \le L_x$ and $z_j = -\cos(\frac{j\pi}{L_z}), 0 \le j \le L_z$, can be approximated as

$$f(x,z) = \sum_{m=0}^{L_x} \sum_{n=0}^{L_z} Gx_m(x) f(x_m, z_n) Gz_n(z), \tag{25}$$

where $Gx_m(x)$ and $Gz_n(z)$ are interpolating functions defined as (24). The partial derivatives of the function $f(x,z)$ at the collocation points may be expressed in the matrix form as:

$$\boldsymbol{F}_{p,q} = \frac{\partial^{p+q}}{\partial x^p \partial z^q} \boldsymbol{F}(x_i, z_j) = \boldsymbol{DX}^p \, \boldsymbol{F}(x_m, z_n) \, \boldsymbol{DZ}^q, \tag{26}$$

where $\boldsymbol{DX}^p$ is $(L_x+1) \otimes (L_x+1)$, $\boldsymbol{F}_{p,q}$ and $\boldsymbol{F}$ are $(L_x+1) \otimes (L_z+1)$ and $\boldsymbol{DZ}^q$ is $(L_z+1) \otimes (L_z+1)$ matrices. The component of $\boldsymbol{DX}$ and $\boldsymbol{DZ}$ may be written as:

$$\boldsymbol{DX}_{i,m} =$$
$$\frac{1}{L_x c_i} \sum_{m=0}^{L_x} \frac{1}{c_m} m \cos(m\pi \frac{L_x - m}{L_x}) \sin(m\pi \frac{L_x - i}{L_x}) / \sin\frac{i\pi}{L_x}, \tag{27}$$

$$\boldsymbol{DZ}_{n,j} =$$
$$\frac{1}{L_z c_j} \sum_{n=0}^{L_z} \frac{1}{c_n} n \cos(n\pi \frac{L_z - n}{L_z}) \sin(n\pi \frac{L_z - j}{L_z}) / \sin\frac{j\pi}{L_z}. \tag{28}$$

The matrices $\boldsymbol{DX}^p$ and $\boldsymbol{DZ}^q$ for the higher derivatives can be obtained by simple matrix multiplications.

The boundary conditions (10) and (11) at the collocation points can be represented by the value of the boundary grids and the outermost internal grids:

$$\text{From} \quad x = \pm 1; \quad \varphi = \frac{\partial \varphi}{\partial x} = \theta = 0,$$
$$\text{yield} \;\; \varphi_{0,j} = \varphi_{L_x,j} = 0, \;\; \theta_{0,j} = \theta_{L_x,j} = 0,$$
$$(0 \le j \le L_z), \tag{29}$$
$$\text{and} \;\; \sum_{m=1}^{L_x-1} \boldsymbol{DX}_{0,m} \varphi_{m,j} = 0; \;\; \sum_{m=1}^{L_x-1} \boldsymbol{DX}_{L_x,m} \varphi_{m,j} = 0;$$
$$(0 \le j \le L_z). \tag{30}$$

Solving equation (30), we can express the outermost internal collocation points in terms of the remaining internal points:

$$\varphi_{1,j} = \sum_{m=2}^{L_x-2} a_m \varphi_{m,j};$$

$$\varphi_{L_x-1,j} = \sum_{m=2}^{L_x-2} b_m \varphi_{m,j}; \quad (0 \le j \le L_z) \tag{31}$$

where

$$a_m = \frac{\boldsymbol{DX}_{0,L_x-1}\boldsymbol{DX}_{L_x,m} - \boldsymbol{DX}_{L_x,L_x-1}\boldsymbol{DX}_{0,m}}{\boldsymbol{DX}_{0,1}\boldsymbol{DX}_{L_x,L_x-1} - \boldsymbol{DX}_{0,L_x-1}\boldsymbol{DX}_{L_x,1}}, \tag{32}$$

$$b_m = \frac{\boldsymbol{DX}_{L_x,1}\boldsymbol{DX}_{0,m} - \boldsymbol{DX}_{0,1}\boldsymbol{DX}_{L_x,m}}{\boldsymbol{DX}_{0,1}\boldsymbol{DX}_{L_x,L_x-1} - \boldsymbol{DX}_{0,L_x-1}\boldsymbol{DX}_{L_x,1}}. \tag{33}$$

Similarly, the boudary conditions;

$$\text{from} \quad z = \pm 1; \quad \varphi = \frac{\partial \varphi}{\partial z} = \theta = 0,$$

$$\text{yield} \ \ \varphi_{i,0} = \varphi_{i,L_z} = 0, \ \ \theta_{i,0} = \theta_{i,L_z} = 0, \quad (0 \le i \le L_x) \tag{34}$$

$$\text{and} \ \ \sum_{n=1}^{L_z-1} \varphi_{i,n}\boldsymbol{DZ}_{n,0} = 0; \ \ \sum_{n=1}^{L_z-1} \varphi_{i,n}\boldsymbol{DZ}_{n,L_z} = 0; \quad (0 \le i \le L_x) \tag{35}$$

$$\varphi_{i,1} = \sum_{n=2}^{L_z-2} c_n \varphi_{i,n}; \ \ \varphi_{i,L_z-1} = \sum_{n=2}^{L_z-2} d_n \varphi_{i,n}; \quad (0 \le i \le L_x) \tag{36}$$

where

$$c_n = \frac{\boldsymbol{DZ}_{L_z-1,0}\boldsymbol{DZ}_{n,L_z} - \boldsymbol{DZ}_{L_z-1,L_z}\boldsymbol{DX}_{n,0}}{\boldsymbol{DZ}_{1,0}\boldsymbol{DZ}_{L_z-1,L_z} - \boldsymbol{DZ}_{L_z-1,0}\boldsymbol{DZ}_{1,L_z}}, \tag{37}$$

$$d_n = \frac{\boldsymbol{DZ}_{2,L_z}\boldsymbol{DZ}_{n,0} - \boldsymbol{DZ}_{1,0}\boldsymbol{DX}_{n,L_z}}{\boldsymbol{DZ}_{1,0}\boldsymbol{DZ}_{L_z-1,L_z} - \boldsymbol{DZ}_{L_z-1,0}\boldsymbol{DZ}_{1,L_z}}. \tag{38}$$

The equations of steady state (14) and linear stability (15) may be discretiziered by the pseudospectral Chebyshev collocation method:

Equation for steady state

$$\boldsymbol{\mathcal{L}}(\boldsymbol{X^s}) = 0, \tag{39}$$

Equation for linear stability

$$\sigma \boldsymbol{B}(\boldsymbol{X^s})\boldsymbol{X'} = \boldsymbol{A}(\boldsymbol{X^s})\boldsymbol{X'}. \tag{40}$$

The equations of steady state (39) are nonlinear equations. On using the direct Newton iterative method, we have:

$$\boldsymbol{\mathcal{J}}(\boldsymbol{X_n^s})\delta\boldsymbol{X} = -\boldsymbol{\mathcal{L}}(\boldsymbol{X_n^s}); \quad \boldsymbol{X_{n+1}^s} = \boldsymbol{X_n^s} + \delta\boldsymbol{X} \tag{41}$$

Coincidentally, the Jacobi matrix $\boldsymbol{\mathcal{J}}(\boldsymbol{X_n^s})$ is identical with matrix $\boldsymbol{A}(\boldsymbol{X^s})$ in equation (40). The matrices $\boldsymbol{A}(\boldsymbol{X^s})$ and $\boldsymbol{B}(\boldsymbol{X^s})$ are almost full matrices, which will be not expressed here. The equations corresponding the boundary grids and outermost internal grids of φ will be overwritten by the boundary conditions (29), (31),(34) and (36).

In our implementation the DGESV routine of LAPACK library[16] is employed for solving the linear equations (41), and the DGGEV routine of LAPACK for the generalized eigenvalue equations(40). The DGESV routine decomposes the Jacobi matrix $\boldsymbol{\mathcal{J}}(\boldsymbol{X_n^s})$ into $\boldsymbol{LU}$. The routine DGGEV reduces $\boldsymbol{A}$ and $\boldsymbol{B}$ to upper triangular form with diagonal elements μ_j and ν_j. The eigenvalues are $\sigma_j = \delta_j + i\omega_j$. Because $\boldsymbol{B}$ matrix is singular, we need to filter out those $\nu_j = 0$ yielded by the QZ algorithm.

The algorithm for calculating the critical Rayleigh number R_H value is the following. As a first step, with parameters Pr, β being given, we choose a R_H value, and solve the equations (41) by Newton iterative scheme. If the Newton iterative is not convergent within limited step, we reduce the R_H and solve the equations (41) again. Next, after having the convergence of $\boldsymbol{X^s}$, we use QZ algorithm to find leading eigenvalue σ_j, which is the largest real part of eigenvalue δ_j among the whole set of eigenvalues of generalized eigenvalues equations(40). Finally, if δ_j is greater than zero, we reduce R_H. If δ_j is less than zero, we increase R_H. We repeat these steps again to find R_H^1 for $\delta_j^1 < 0$ and R_H^2 for $\delta_j^2 > 0$. Between R_H^1 and R_H^2, we search the critical Rayleigh number R_H by bisection method such that corresponding δ_j approaches zero.

4 Discussion of Results

First we check the influence of grid's resolution. The grid resolutions (16×16),(20×20) and (32×20) are analyzed for $Pr = 10$, $\beta = 1, 2, 4, 8, 12, 16, 20, 50$. Fig. 2, show the results of critical R_H. We note that grid's resolution has a great influence on the accuracy of critical R_H values. But the feature of critical R_H in relation to the aspect ratio is almost similar. The computer time consumption will dramatically increase as grid's resolution becomes finer. For $\beta = 50$, and grid's resolution 32×20, we have $R_H = 13081.8$. It is almost close with linear result $R_H = 15504.8$. We thus adopt (32×20) grid's resolution for our further analysis because it is a reasonable compromise between accuracy and computer time.

Imberger[8], Cormack, Leal and Seinfeld[13] have investigated the shallow cavity with differentially heated end walls through experiment and numerical analysis. They showed that flow structure in the core region is simply a parallel flow. Hart[1] gave the simple basic flow for the infinite case. According to our nondimensional scheme, the basic flow is:

$$u^s = \frac{R_H}{48} z(1 - z^2), \tag{42}$$

$$\theta^s = \frac{R_H^2}{11520}(7z - 10z^3 + 3z^5). \tag{43}$$

We compare the steady velocity and temperature solutions of numerical simulation with analytical results (42)

and (43). Fig.3 show the streamline of φ^s and steady isoline of temperature solution θ^s for $Pr = 10$, $\beta = 50$, $R_H = 500$. Apart from near the walls, they show simply parallel flow patterns. Fig. 4 shows the profiles of velocity u^s and θ^s at $x = 0$ determined numerically. They show that results are almost identical between numerical analysis and analytical expressions (42) and (43). This gives confidence to our numerical approach. If we increase the Rayleigh number R_H, the steady flow pattern has a dramatical change. Fig. 5 shows the streamline and isoline of temperature θ^s for $Pr = 10$, $\beta = 16$, $R_H = 6000$. It is interesting to note that the Kelvin cat's eye pattern appears for the steady flow. If the aspect ratio β and Rayleigh number R_H are relatively large, the Kelvin cat's eye pattern of the steady flow will appear in most cases for R_H far below critical R_H values. For the case of $Pr = 10$, $\beta = 30$, Fig.6 show the isoline for gradually increasing R_H values. We note that a significant change of flow pattern occurs between $R_H = 2800$ and $R_H = 3200$.

The effect of β, the aspect ratio, for different Pr values $(100, 10, 1, 0.027)$ on the critical R_H values is presented in Table 1. We note that the flow is more stable at higher Pr values and also when the aspect ratio is small. For all Pr values the flow appears destabilizing as β increases. This fact is corroborated in Fig. 7, where isolines of stream function and temperature are plotted for $Pr = 10$. We note from these figures that beyond $\beta = 16$, the cells appear significantly distorted and the flow becomes multicellular. At the present time, we can identify the cat's eye flow pattern only by plotting the streamlines. Finally in fig 8, we try to elucidate the secondary flow pattern. Here the real part of the leading eigenfunctions for both stream function and the temperature are plotted for $Pr = 10$. It is interesting to note from these figures, that how the flow and temperature pattern becomes gradually complicated as the aspect ratio increases. Above $\beta = 16$, we note the anticipated oscillatory type behaviour. In conclusion we have, in the present note, shown that by judiciously applying the Chebyshev pseudo-spectral method, one can obtain significant results within a reasonable computer time.

Acknowledgments

The work reported in this paper has been supported by the Grant NO. A7728 of NSERC of Canada. The authors gratefully acknowledge the support thus received.

REFERENCES

[1] Hart,J.E.: J. Atmos. Sci. 29 (1972) 687-697

[2] Hart,J.E.: J. Fluid Mech. 132 (1983) 271-281

[3] Hadley, G.: Phil. Tran. Roy. Soc. London 29 (1935) 58-62

[4] Kuo,H. and Korpela, S. A.: Phys. Fluids 31 (1988) 33-42

[5] Wang, T.M. and Korpela, S. A.: Phys. Fluids A 1(6) (1989) 947-953

[6] Laure, P. and Roux B.: C.R.A.S. Series II, Tome 305, (1987) 1137-1143

[7] Daniels,P.G., Blythe,P.A. and Simpkins, P.G.: Proc. R. Soc. London A 411 (1987) 327-350

[8] Imberger, J.: J. Fluid Mech. 65 (1974) 247-260

[9] Ostrach,S., Loka, R.R. and Kumer, A.: 19th Nat. Heat Trans. Conf. Orlands A.S.M.E. Heat Transfer Division vol. 8 (1980) 1-10

[10] Simpkins,P.G. and Dudderar,T.D.: J. Fluid Mech. 110 (1981) 433-456

[11] Hung, M.C. & Andereck, C.D.: Physics letters A 132 Oct. 1988 253-258

[12] Drummond, J. and Korpela, S. A.: J. Fluid Mech. vol 182 (1987) 543-564

[13] Cormack, D.E., Leal,L.G. and Steinfeld, J.H.: J. Fluid Mech. 65 (1974) 231-246

[14] Park, H.M. & Ryu, D.H.: J. Non-newtonian Fluid Mech. 98 (2001) 169-184

[15] Canuto, C., Hussaini, M.Y., Quarteroni, A. & Zang, T.: *Spectral Methods in Fluid Dynamics* 1988 Springer

[16] Anderson, E. and Bai, Z. and Bischof, C. and Blackford, S. and Demmel, J. and Dongarra, J. and Du Croz, J. and Greenbaum, A. and Hammarling, S. and McKenney, A. and Sorensen, D.: *Lapack User's Guide* Society for Industrial and Applied Mathematics (1999), ISBN 0-89871-447-8

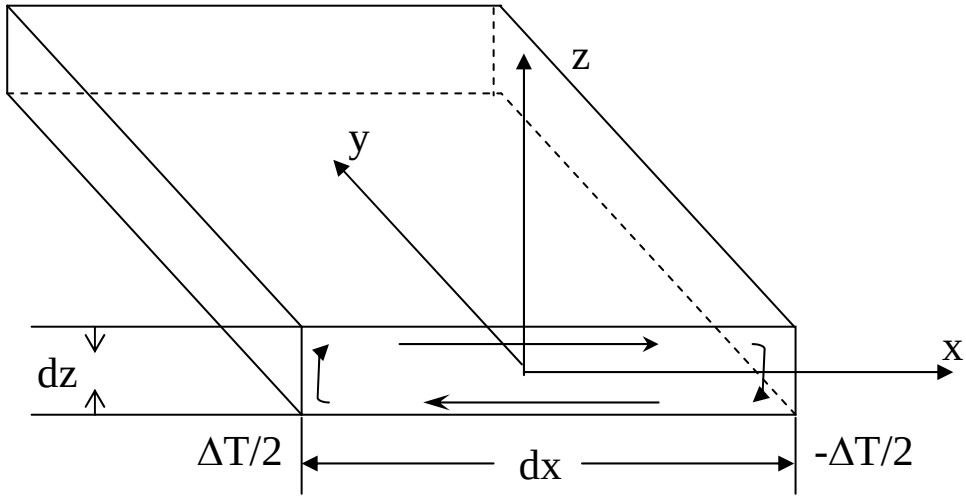

Fig.1 Basic geometry and the coordinate system

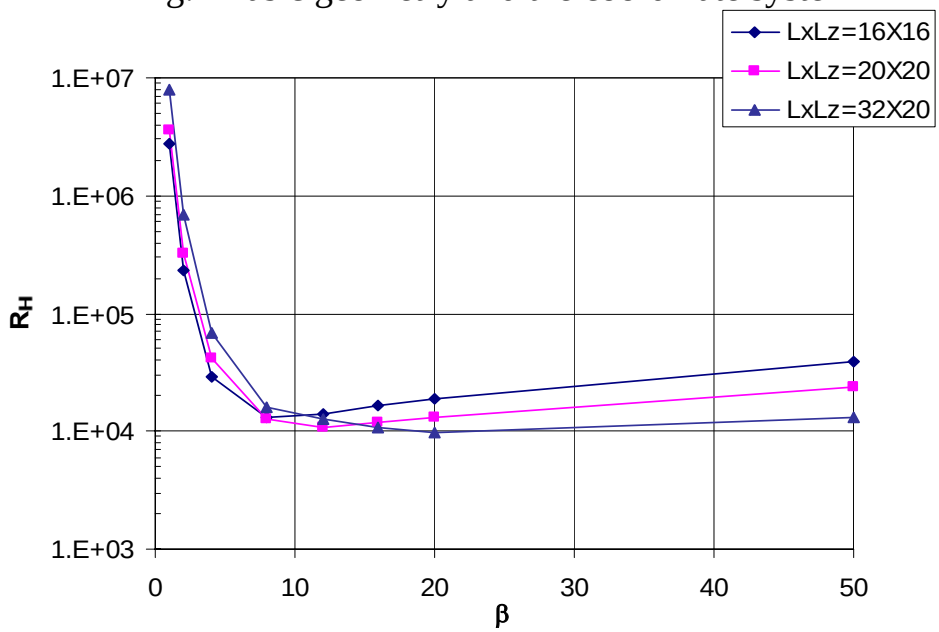

Fig 2. Critical R_H values for Pr=10

Pr	β	1	2	4	8	12	16	20	50	∞*
100	R_H	8921000	703342.0	70970.2	15933.8	12561.8	11341.9	10281.0	12939.0	15372.2
	ω	10311.3	2820.5	1036.0	513.2	363.1	411.4	334.9	222.6	850.0
10	R_H	7971620	700313.0	68808.1	15781.5	12595.8	10609.9	9784.8	13081.8	15504.6
	ω	8113.1	2411.9	1201.0	448.1	443.2	342.1	278.5	204.7	832.3
1	R_H	1966500	271453.0	57890.6	23031.7	14808.1	12213.1	11103.5	10101.6	20103.2
	ω	1906.2	735.5	374.9	486.2	409.8	310.3	252.0	133.6	1026.8
0.027	R_H	70734.4	14948.6	869.2	1544.1	285.0	220.6	219.6	300.0	227.8
	ω	220.8	43.8	3.2	3.5	0.0	0.0	0.0	0.0	0.0

Table 1 Critical R_H values for different Pr

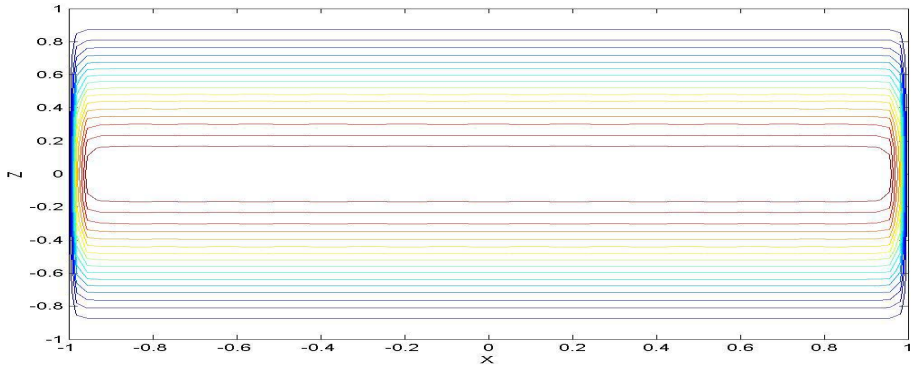

Fig.3 (a) Streamline (Pr=10,β=50 R_H=500)

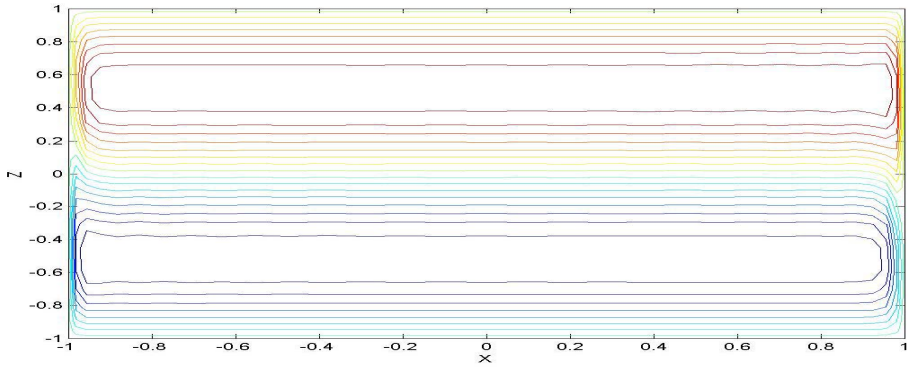

Fig.3 (b). Isoline of Temperature θ (Pr=10, β=50 R_H=500)

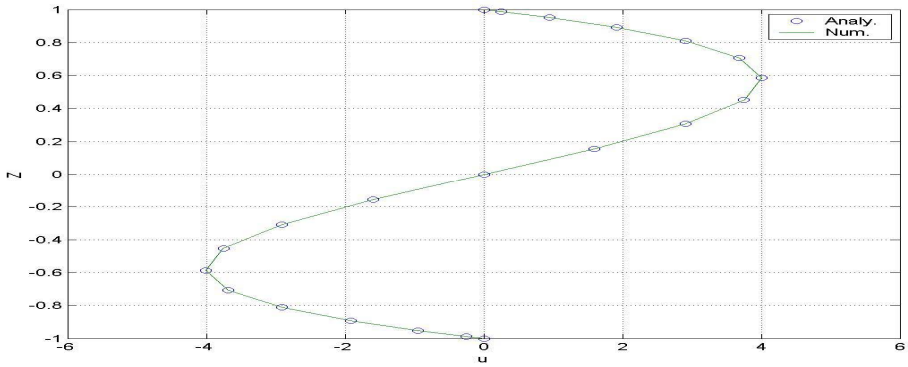

Fig . 4(a) Velocity U at x=0 (Pr=10, β=50 R_H=500)

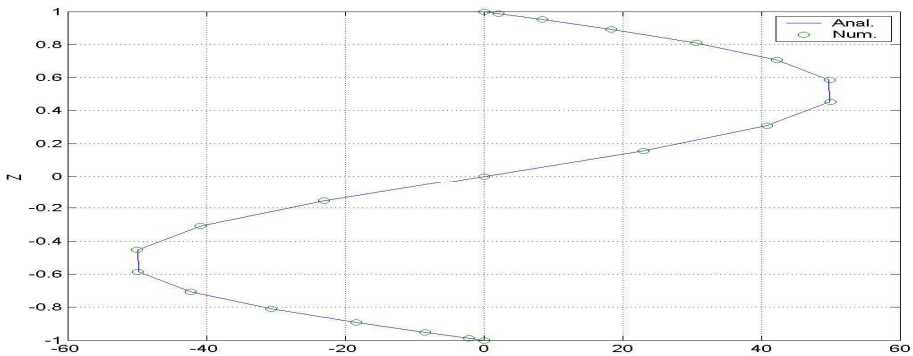

Fig.4(b) Temperature θ at x=0 (Pr=10, β=50 R_H=500)

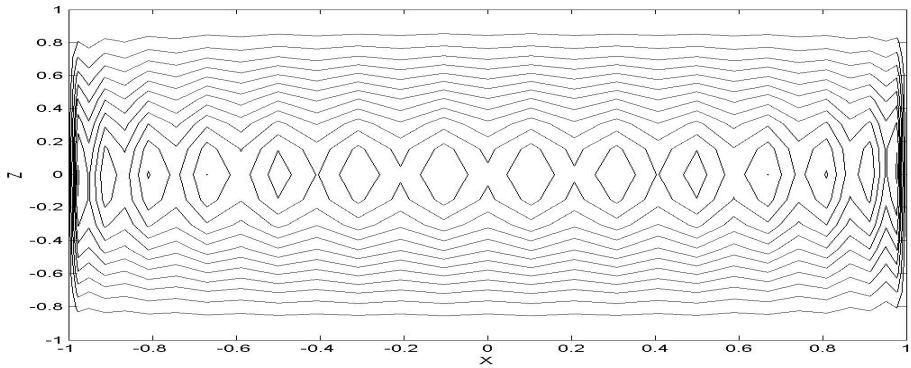

Fig. 5(a) Streamline (Pr=10,β=50 R_H=6000)

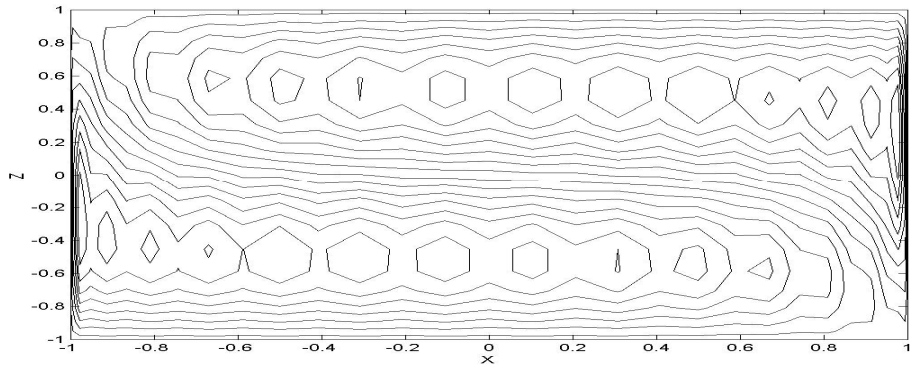

Fig.5(b) Isoline of Temperature θ (Pr=10, β=50 R_H=6000)

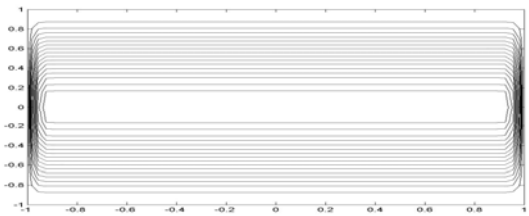

(a) R_H= 200

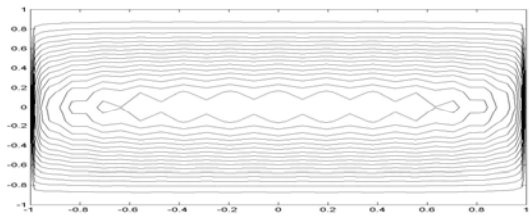

(c) R_H= 4000

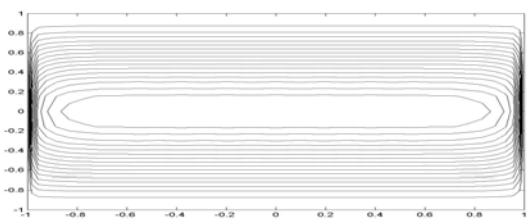

(b) R_H= 2000

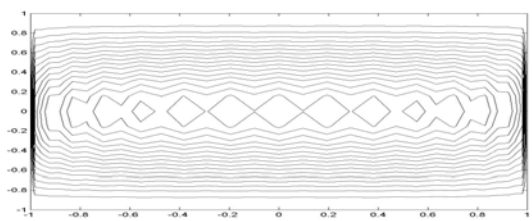

(d) R_H= 5400

Fig.6 Isoline of stream function of Steady flow (Pr = 10.0,β=30)

Isoline of streamfunction

Isoline of temperature θ

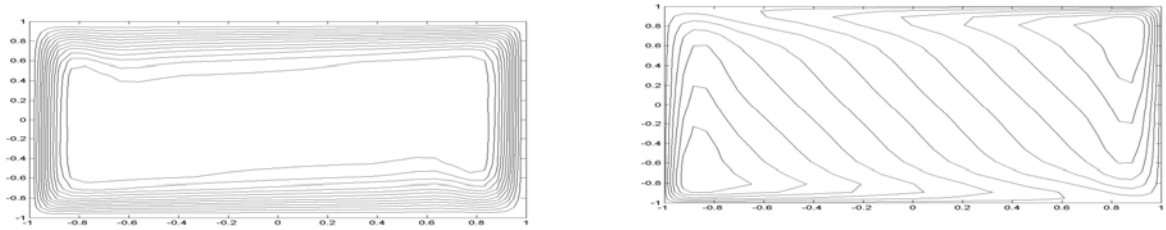

(a) β=1,R_{HC}= 7916730.0

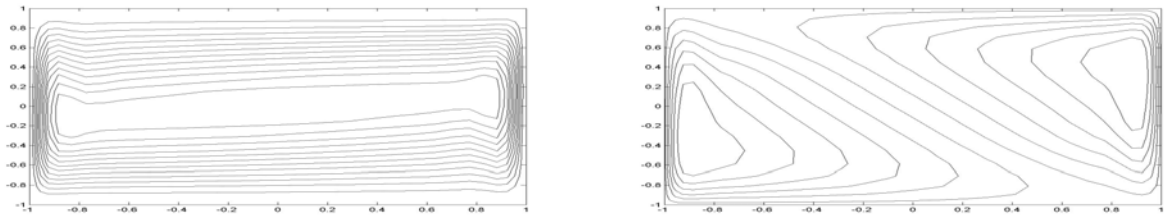

(b) β=4,R_{HC}= 77546.3

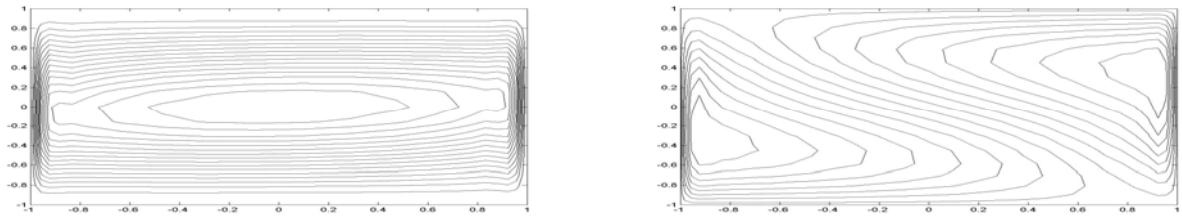

(c) β=8,R_{HC}= 16270.4

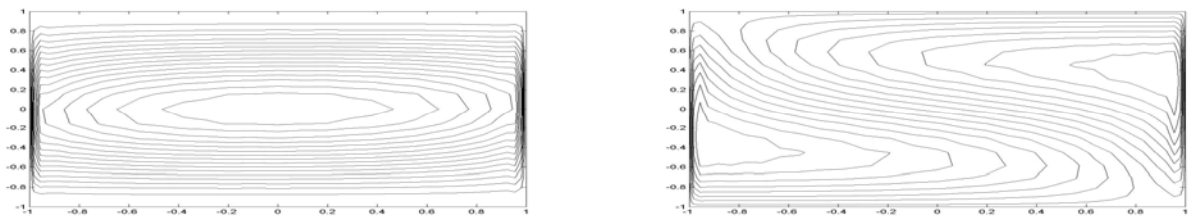

(d) β=16,R_{HC}= 11074.5

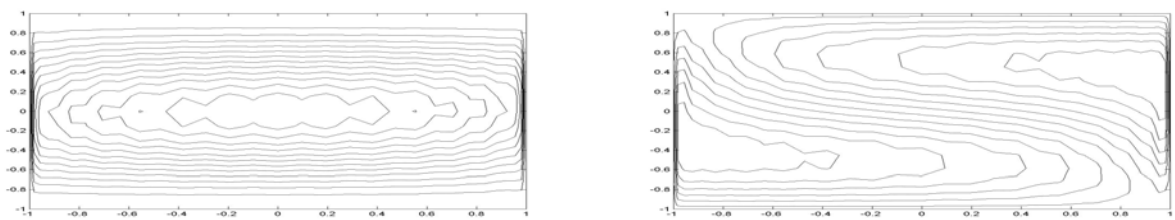

(e) β=20,R_{HC}= 10066.4

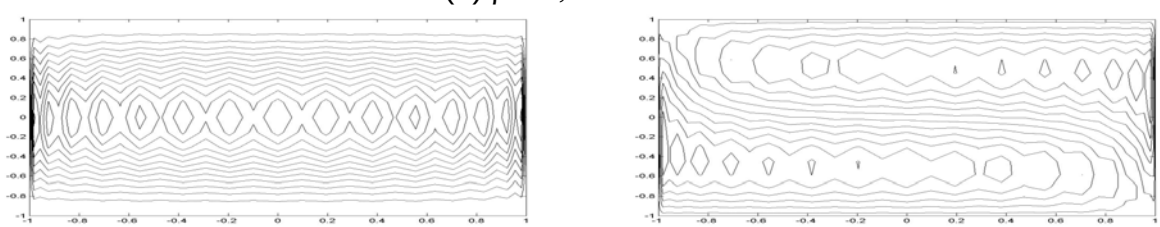

(f) β=50,R_{HC}= 12141.0

Fig. 7 Steady flow , Pr = 10.0

Isoline of streamfunction | Isoline of temperature θ

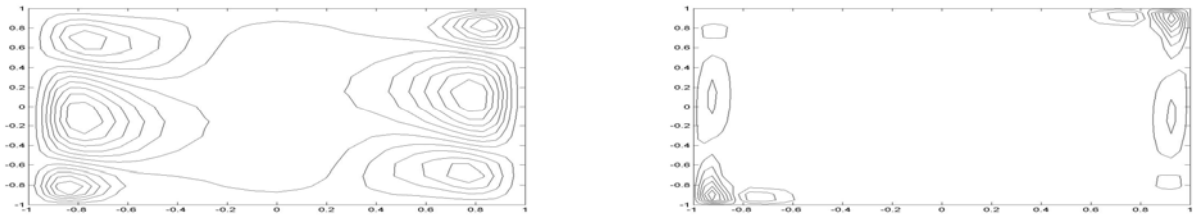

(a) β=1,R_{HC}= 7916730.0

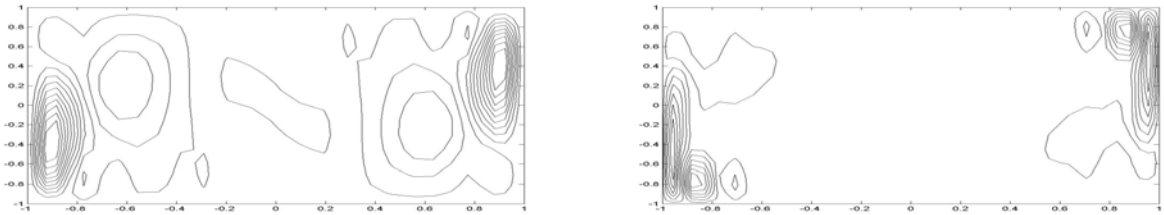

(b) β=4,R_{HC}= 77546.3

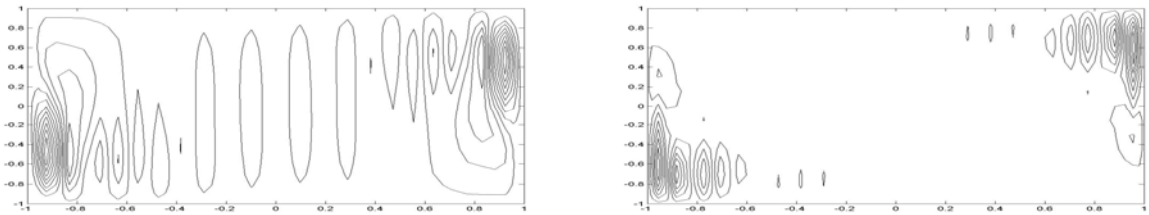

(c) β=8,R_{HC}= 16270.4

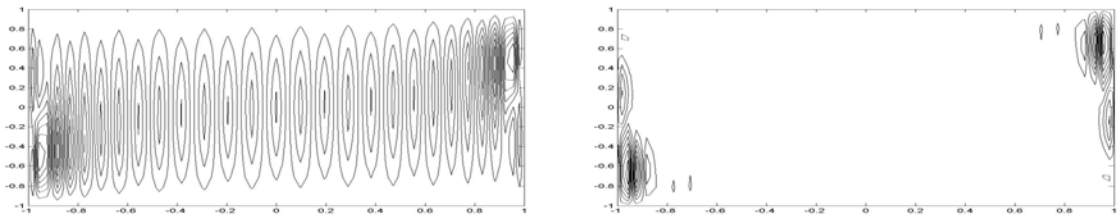

(d) β=16,R_{HC}= 11074.5

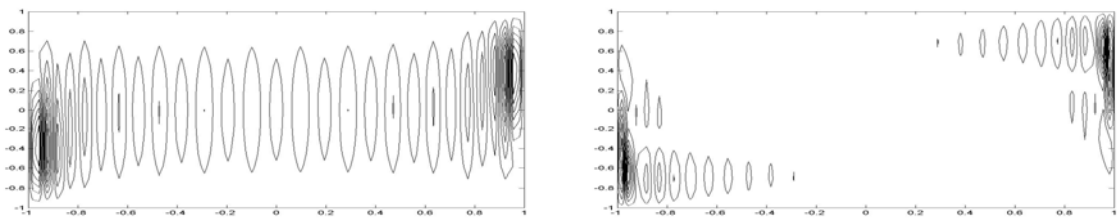

(e) β=20,R_{HC}= 10066.4

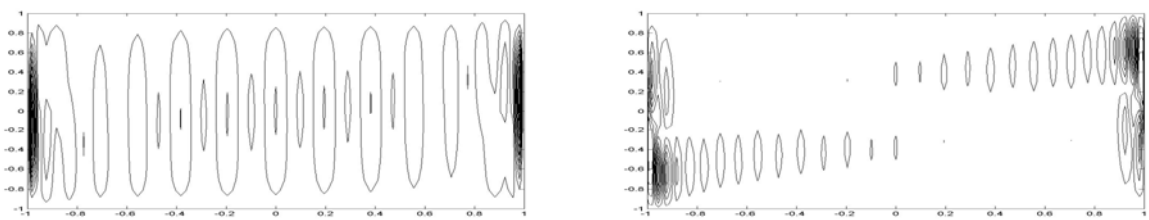

(f) β=50,R_{HC}= 12141.0

Fig.8 Realparts of leading Eigenfunctions (Pr = 10)